Journal of Structural Geology 30 (2008) 1013–1023

Contents lists available at ScienceDirect

Journal of Structural Geology

journal homepage: www.elsevier.com/locate/jsg

Numerical modelling of the effect of matrix anisotropy orientation on single layer fold development

Thomas Kocher [1], Neil S. Mancktelow*, Stefan M. Schmalholz

Geologisches Institut, ETH Zürich, Sonneggstrasse 5, CH-8092 Zürich, Switzerland

ARTICLE INFO

Article history:
Received 22 November 2007
Received in revised form 7 April 2008
Accepted 15 April 2008
Available online 29 April 2008

Keywords:
Planar anisotropy
Single layer folds
Asymmetric folds
Numeric modelling
Finite element modelling
Viscous flow

ABSTRACT

The influence of matrix anisotropy of variable orientation on single layer folding is investigated using finite element models. Both linear (Newtonian) and power-law viscous materials are considered. The results show that the available isotropic analytical solution, when modified to include an appropriate approximation for the anisotropic viscosity, accurately predicts growth rates at small amplitude for planar anisotropy oriented at $\alpha = 45^\circ$ to the competent layer for a wide range of normal viscosity ratios between single layer and matrix ($\mu_c = 10, 100$) and degrees of anisotropy (δ = normal viscosity/shear viscosity = 2, 12, 25). For high normal viscosity ratio ($\mu_c = 100$), the deviation from the analytical solution for other orientations increases with increasing degree of anisotropy but still remains relatively small (<5% for $\delta = 25$). For low normal viscosity ratio ($\mu_c = 10$), the differences for high δ are more significant and for $\alpha \neq 0^\circ$, 45°, or 90° also depend on the imposed boundary conditions. However, if carefully applied, the analytical solution does provide a benchmark test for numerical codes that include oblique anisotropy. The numerical models at both small and finite amplitude show that a tight control on the boundary conditions is crucial for experiments with anisotropic materials, especially when the anisotropy is oblique to the boundaries. Analogue experiments with anisotropic materials, where boundary conditions are more difficult to control, must therefore be designed and interpreted with caution. Matrix anisotropy initially oriented obliquely with regard to the maximum shortening direction results in asymmetric buckle folds in the single layer and asymmetric chevron folds in the matrix, even if the deformation is purely coaxial. This is true for both linear and power-law materials and for a range of boundary conditions, both free and constrained. Asymmetric natural fold structures in anisotropic material do not therefore necessarily imply a component of non-coaxial flow.

1. Introduction

As shown in an earlier study (Kocher et al., 2006), layer-parallel anisotropy in the matrix has a strong influence on the infinitesimal and large amplitude stages of single layer folding. The occurrence of an internal instability in the matrix (e.g. Biot, 1965; Cobbold et al., 1971; Cobbold, 1976; Latham 1985a,b; Fletcher, 2005), and its interference with the single layer of higher viscosity, cause substantial changes in growth rates, dominant wavelengths, amplification history, and finite structure pattern compared to an isotropic material. In this previous study, we specifically considered the situation where a pre-existing planar anisotropy is fixed to material points from the onset of deformation and initially parallel to an embedded, more competent single layer. Natural examples would be finely layered sedimentary rocks, such as turbidites or radiolarites, or metamorphic rocks with a strong foliation or banding developed due to metamorphic segregation. In these cases, the bulk anisotropic behaviour reflects the stacking of layers with different viscosities or a set of closely-spaced slip surfaces (corresponding to the "IMSS fluid" of Fletcher, 2005; see also Cobbold et al., 1971). The anisotropy therefore remains parallel to the layer boundaries during subsequent deformation if the material distribution is not altered by metamorphic or metasomatic processes. Because multilayered rocks are common in nature, this is an important case to consider in detail. However, it is only one end-member of a more general situation, where both the degree of the anisotropy and its orientation relative to the layer may vary both initially and during deformation. For example, the approximately planar foliation in natural slates and schists is typically oblique to bedding or layering. In polydeformed terrains, subsequent deformation leads to a crenulation or kinking of the foliation and to second-phase folding of the layering. In this case, the obliquity of the foliation may be expected to influence the dynamics of buckling and the geometry of folds developed in the layering.

* Corresponding author.
E-mail address: neil.mancktelow@erdw.ethz.ch (N.S. Mancktelow).
[1] Present address: Shell International Exploration and Production B.V., Kesslerpark 1, 2288 GS, Rijswijk, The Netherlands.

0191-8141/$ – see front matter © 2008 Elsevier Ltd. All rights reserved.
doi:10.1016/j.jsg.2008.04.006

In this paper, finite element models are used to consider pure shear deformation of an isotropic competent layer embedded in a rock matrix with differing initial degrees of planar anisotropy and differing initial orientations of this planar anisotropy relative to the layer. Both Newtonian and non-linear (power-law) viscous materials are considered. In particular, it is investigated: (1) if the analytical theories of Fletcher (1974) and Smith (1977) can still be applied to determine growth rates and dominant wavelengths; (2) if oblique anisotropy might cause asymmetric folds to develop in a background flow field of pure shear; and (3) the influence of oblique anisotropy on the matrix deformation processes.

2. Numerical method

The numerical experiments were performed using the finite element code FLASH (Kocher, 2006) and an equivalent code of Mancktelow (e.g. Viola and Mancktelow, 2005; Passchier et al., 2005), which solve the Stokes equations in combination with a non-linear anisotropic power-law rheology in the absence of gravity. Nine-node quadratic elements for velocity discretization are combined with a linear pressure approximation (three degrees of freedom) to avoid chessboard patterns in pressure fields (e.g. Cuvelier et al., 1986; Poliakov and Podladchikov, 1992). The implementation of anisotropic viscosity in these codes follows Mühlhaus et al. (2002a,b; their Eq. (8) in both publications), as outlined in Kocher (2006) and Kocher et al. (2006, Appendix A). To verify the results, both codes were tested on a number of model setups for which analytical solutions are available, including the analytical solutions of Fletcher (1974) for folding in linear and non-linear viscous material, and Schmid and Podladchikov (2003) for the stress and strain rate fields around an elliptical inclusion in Newtonian fluids.

3. Influence of anisotropy orientation on growth rate spectra of single layer folds

The analytical solutions of Fletcher (1974) and Smith (1975, 1977) predict the growth rates and dominant wavelengths of single layer folds in power-law viscous material at infinitesimal amplitudes. These two independent analytical derivations give equivalent results for the growth rate spectra and here the equation of Fletcher (1974) is used. In Kocher et al. (2006), it was demonstrated that this analytical solution also allows the determination of growth rates for layers embedded in a linear viscous anisotropic matrix. This solution makes use of a proposal by Biot (1965) that the bulk viscosity of an infinite anisotropic half-space can be approximated by $\mu = \sqrt{\mu_n \mu_s}$, where μ_n and μ_s are the normal and shear viscosity of the material. The resulting analytical growth rate was shown to be in good, though not perfect, agreement with the results obtained from finite element analysis (max. error $\leq$5% for the chosen parameters, cf. Fig. 2d of Kocher et al., 2006).

However, it has not yet been established if the analytical solution for growth rates in anisotropic material also applies to the more general case of a non-layer parallel anisotropy orientation. To check this, growth rate spectra of a single isotropic Newtonian layer embedded in an anisotropic Newtonian matrix were calculated for a normal viscosity contrast of $\mu_c = 10$ and 100. For each of three degrees of anisotropy ($\delta = \mu_n/\mu_s = 2, 12$, and 25), growth rate values were calculated for an angle between the competent layer and the plane of anisotropy of $\alpha = 0°$, 20°, 45°, 70° and 90°.

The resulting growth rate spectra are shown in Fig. 1. The following observations can be made from these plots. (1) The numerical results are symmetrical about an anisotropy inclination of 45° to the competent layer. For example, the growth rates for an anisotropy oriented at 0° and 90° or at 20° and 70° to the layer are identical because these orientations are equally inclined relative to the 45° orientation. This is to be expected because the constitutive (or material) operator relating stress to strain rate in the anisotropic matrix is symmetric (Mühlhaus et al., 2002a,b; Kocher et al., 2006, Appendix A) and therefore insensitive to a switch in axes (equivalent to a reflection across the 45° orientation). (2) The analytical solution of Fletcher (1974) is best approximated by the numerical results if the anisotropy is oriented at 45° to the competent layer. (3) The numerical results for $\alpha = 0°$ or 90° – for which the analytical solution was initially proposed – show a good fit to the predicted analytical values for high viscosity contrast (e.g. $\mu_c = 100$ in Fig. 1a–c). (4) Overall, the model growth rates increasingly deviate from the analytical curve with increasing degree of anisotropy but, for high viscosity contrast ($\mu_c = 100$), the maximum deviation still remains relatively small (<5% for $\delta = 25$ and $\alpha = 20°$ or 70° in Fig. 1c). (5) For $\alpha \neq 45°$, the fit of the numerical results to the analytical solution deteriorates with decreasing normal viscosity contrast between matrix and layer (e.g. $\mu_c = 10$ in Fig. 1d–f). (6) The growth rates for $\alpha = 0°$ or 90° are generally lower than the theoretical curve, whereas those for $\alpha = 20°$ or 70° are higher (at least for the boundary conditions of Fig. 1, see below).

Fig. 2 shows a curve of the maximum growth rate as a function of the angle α between the plane of anisotropy and the single layer, for the same boundary conditions and material properties ($\mu_c = 10$, $\delta = 25$) as is in Fig. 1f. The expected reflection symmetry about the 45° direction is immediately obvious, with a maximum in the growth rate at $\alpha \approx 12.5°$ and 77.5°. These results indicate that, with free slip allowed on the side boundaries, the maximum initial growth rate of the single layer fold occurs when the planar anisotropy is only slightly oblique. However, the outcome is strongly influenced by the applied boundary conditions.

In Fig. 3, the effects of changing boundary conditions on the growth rate at very small fold amplitude are investigated, with a setup otherwise equivalent to Fig. 1f. For upper and lower model limits that are far removed from the central layer (for Figs. 1–3, the height of the model is eight times the width), a change in the upper and lower boundary conditions from (1) free slip in the x direction but prescribed v_y, to (2) totally prescribed v_x and v_y, has no effect on the growth rate. In run (3), the upper and lower boundaries were fully prescribed as in (2) but v_y was also set to zero at the inflection points on the mid-line of the initial sinusoidal perturbation in the single layer. This effectively ensures that the single layer itself cannot rotate. As can be seen from Fig. 3, this has no effect on the growth rates, even when the anisotropy in the matrix is oblique to the layer and to the boundaries (e.g. for $\alpha = 20°$ or 70°). In contrast, modifying the side boundary conditions does have a significant influence on the fold growth rate for orientations other than $\alpha = 0°$, 45°, or 90°. If, rather than allowing free slip, v_y on the sides is constrained to be periodic (by assigning only a single global degree of freedom in v_y to every pair of corresponding nodes on either side), the growth rate for $\alpha = 20°$ or 70° is significantly lower, as seen for (4) and (5) in Fig. 3, whereas there is no change for $\alpha = 0°$, 45° or 90°. There is thus a markedly different response depending on whether the single layer alone is constrained to not rotate (no significant effect) or both the layer and anisotropic matrix are constrained to have no component of bulk rotation (leading to a reduction in growth rate).

In summary, the numerically calculated growth rate spectra show that in general the initial growth rates depend strongly on the orientation of the anisotropy plane with respect to the competent layer (Fig. 2), although the influence decreases for higher normal viscosity contrast between layer and matrix (Fig. 1). However, as was previously shown in Kocher et al. (2006), the geometry and kinematics of finite-amplitude folding is also influenced by matrix deformation processes, such as the formation of kink-bands or chevron folds, and these effects are not considered in the infinitesimal amplitude analytical solutions nor in the corresponding numerical models of Figs. 1–3.

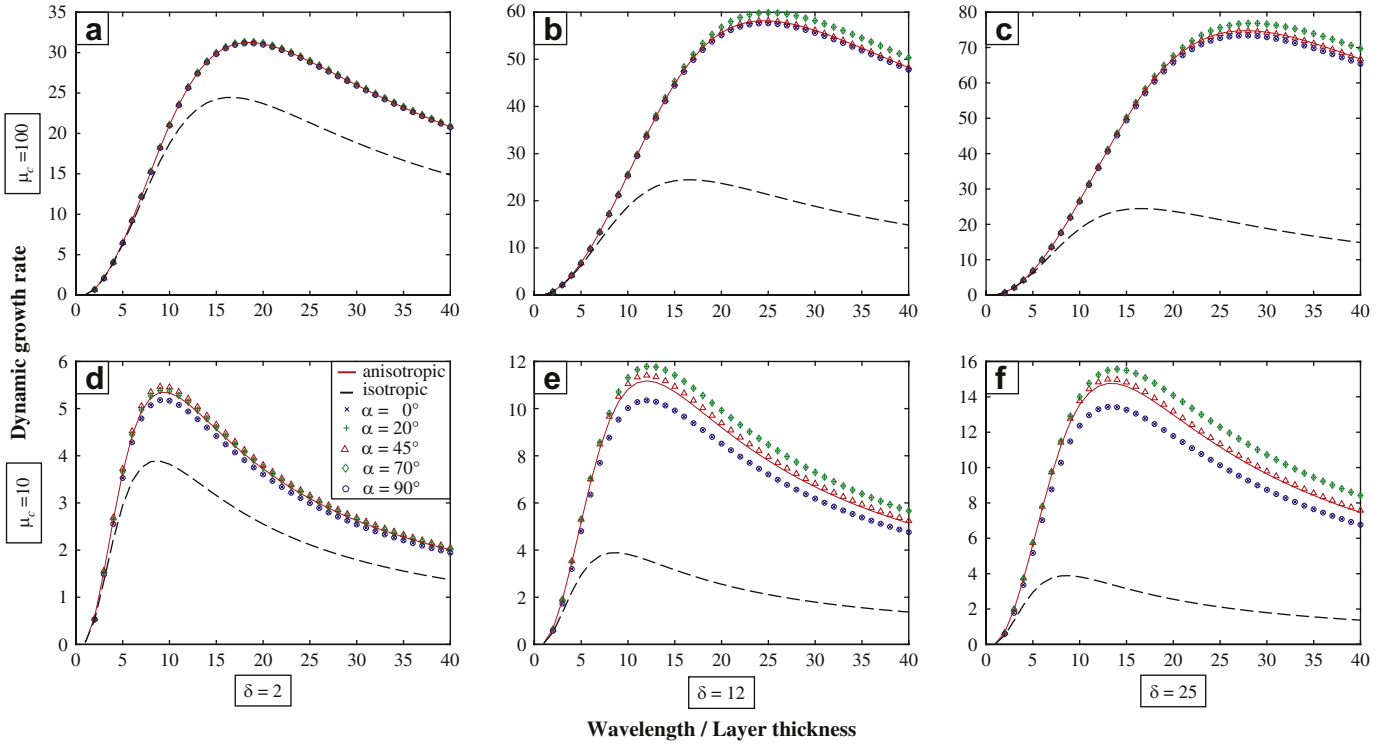

Fig. 1. Dynamic growth rate spectra of folds for a Newtonian (i.e. linear viscous) isotropic single layer embedded in a Newtonian anisotropic matrix with different anisotropy orientations, for normal viscosity contrasts of $\mu_c = 10$ and 100. α describes the difference in orientation between the competent layer (which is parallel to the maximum shortening direction) and the plane of anisotropy, i.e. if $\alpha = 90°$, the anisotropy is oriented perpendicular to the competent layer. The height of the models is eight times the width, v_x and v_y are both prescribed on the upper and lower boundaries, whereas only v_x is prescribed on the side boundaries ("free slip" in the y direction). The initial perturbation is sinusoidal with an amplitude A_0 equal to 10^{-3} of the layer thickness. The width of the model corresponds to one wavelength, with the side boundaries coincident with the hinge position. The dynamic growth rate is determined for the central hinge from the average of the amplitude A at the upper and lower boundaries of the layer as $q = \log_e(A/A_0)/\varepsilon_{xx} - 1$, where the strain increment ε_{xx} in the x direction parallel to the layer is 10^{-5}. The dashed curve is the same in all figures and corresponds to the isotropic analytical solution of Fletcher (1974). The solid curve is the same analytical solution but with the viscosity in the matrix approximated by $\mu = \sqrt{\mu_n \mu_s}$, where μ_n and μ_s are the normal and shear viscosity of the material. The degree of anisotropy is given by $\delta = \mu_n/\mu_s$.

4. Anisotropy orientation effects on finite fold formation

To explore the influence of planar anisotropy of arbitrary orientation on the finite development of a single layer fold, a Newtonian isotropic layer was subjected to pure shear deformation in a Newtonian anisotropic matrix material for differing degrees of anisotropy and differing orientations. The viscosity contrast

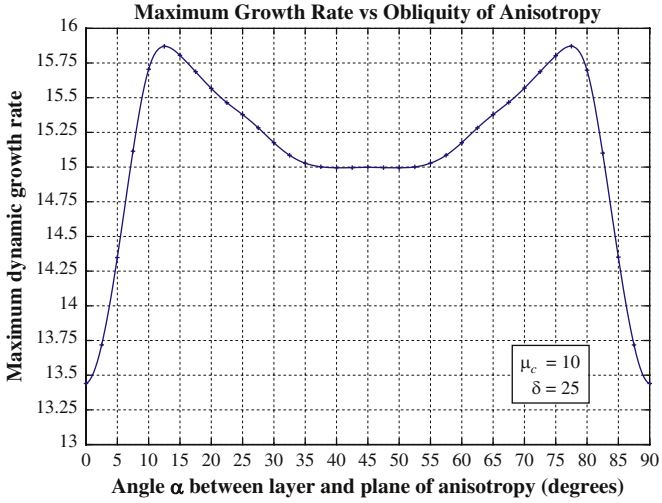

Fig. 2. Variation in the maximum dynamic growth rate as a function of the angle of obliquity α between the plane of anisotropy and the single layer for the parameters of Fig. 1f.

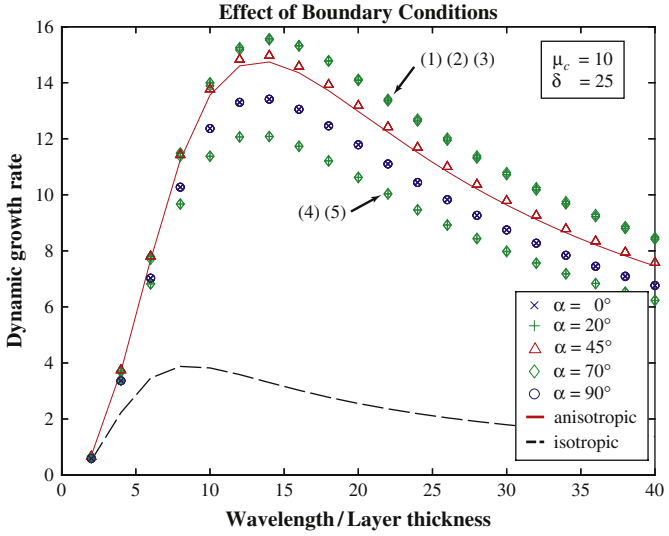

Fig. 3. Dynamic growth rate spectra corresponding to Fig. 1f for different boundary conditions. (1) Prescribed v_y but unconstrained v_x ("free slip") on the upper and lower boundaries, constrained v_x and unconstrained v_y ("free slip") on the side boundaries; (2) both v_x and v_y prescribed on the upper and lower boundaries, same boundary conditions on the sides as in (1); (3) both v_x and v_y prescribed on the upper and lower boundaries, and v_y set to zero at the two inflection points of the initial sinusoidal perturbation, same boundary conditions on the sides as in (1); (4) prescribed v_y but unconstrained v_x ("free slip") on the upper and lower boundaries, v_y at the left and right sides constrained to be equal ("periodic" boundary conditions in v_y); (5) both v_x and v_y prescribed on the upper and lower boundaries, and v_y periodic at the left and right sides.

between layer viscosity and matrix normal viscosity was set to 10, which would result in very low growth rates in an isotropic Newtonian matrix (and can be shown in numerical experiments to be too small to form folds with large wavelength to thickness ratios). The layer interface was perturbed with a sinusoidal initial perturbation with wavelength equal to the dominant wavelength calculated from the analytical solution of Fletcher (1974) for an isotropic matrix and with a maximum amplitude equal to 5% of the layer thickness. Free surface boundary conditions were applied at the top boundary. All other boundary velocities were prescribed except for the lateral boundaries, where the vertical velocity v_y was set to be periodic, but otherwise unconstrained. The resulting folds and the matrix anisotropy orientation after 32% bulk shortening are shown in Figs. 4 and 5.

A layer-perpendicular anisotropy has no influence on the fold symmetry irrespective of the degree of anisotropy (Fig. 4a1–a3). The anisotropy influences the growth rate of the folds, but since the growth rates are small due to the small normal viscosity contrast between layer and matrix, the differences in finite amplitude are barely noticeable. If the anisotropy deviates slightly from a perpendicular orientation (Fig. 4b1–b3), the developing fold is no longer symmetrical and shows two wavelengths: a short one that is determined by the wavelength of the initial perturbation, and a long one for which the layer is folded into an asymmetric shape. For the imposed side boundary conditions (straight with periodic v_y), the wavelength of any fold developed must be an integer fraction of the model width (1, ½, etc.) and in this case the wavelength of the large fold appears to be determined by the model width itself. Although the amplitude of the fold with this second longer wavelength is large, there is little evidence of strong matrix deformation in the form of rotated planes of anisotropy, as might be expected to form for such large amplitude in an isotropic matrix. Without additional markers (also generally absent in finely foliated natural phyllites or schists), it is therefore difficult to visualize the extent of deformation in the matrix, as a cleavage-parallel shearing causes no deflection of the cleavage planes themselves.

For $\alpha = 45^\circ$ (Fig. 5a1–a3), the folds in the competent layer are again symmetric, and no second wavelength folding is observable. The matrix deformation is localized close to the competent layer, as shown by the small areas near the competent layer where the anisotropy is rotated. An increase in the degree of anisotropy within the matrix causes a very small increase in fold amplitude, but no significant asymmetry of the fold train itself.

However, if the planar anisotropy in the matrix is sub-parallel to the layer ($\alpha = 20^\circ$ in Fig. 5b1–b3), the finite geometry of both matrix and layer looks remarkably different. Asymmetric chevron folds occur in the matrix, which merge into a single larger chevron structure with increasing degree of anisotropy δ (Fig. 5b2–b3). The single competent layer is folded on two wavelengths. The shorter wavelength folding is determined by the wavelength of the initial perturbation, whereas the longer wavelength folding, whose amplitude increases with increasing degree of anisotropy, has a wavelength

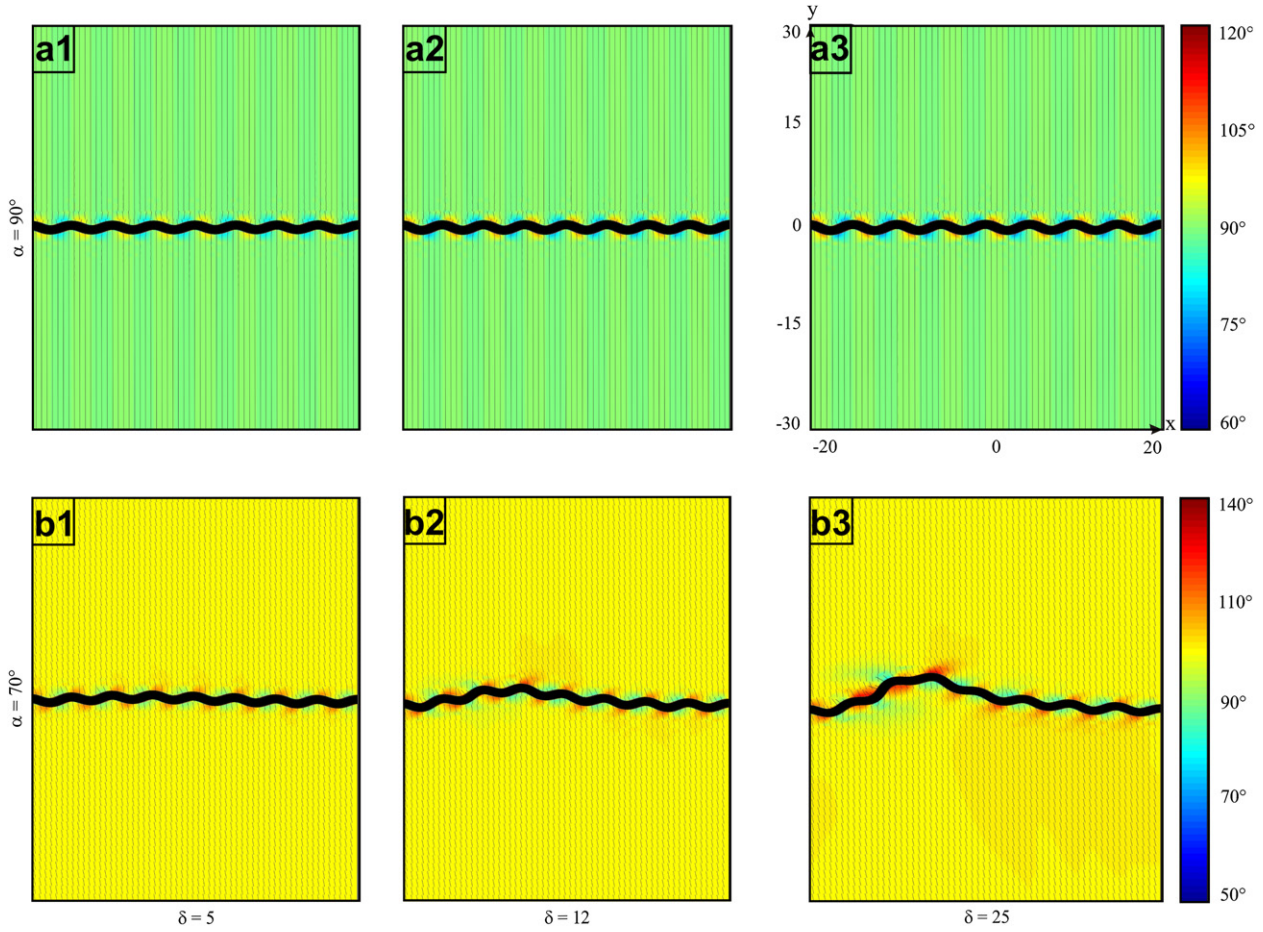

Fig. 4. Colour-coded plots of the orientation of the anisotropy planes and the finite fold shape after 32% of layer-parallel pure shear shortening in a Newtonian material (normal viscosity contrast $\mu_c = 10$), for matrix anisotropy degrees of $\delta = 5$, 12 and 25. For the colour code, positive angles are measured anticlockwise from the x-axis. α denotes the initial clockwise difference in orientation between the competent layer and the anisotropy plane. (a1–a3): initial anisotropy orientation perpendicular to the competent layer ($\alpha = 90^\circ$); (b1–b3): anisotropy initially oriented at 70° (sub-perpendicular) to the layer. The thin black lines trace the planes of anisotropy in the matrix. At the lower boundary v_x and v_y are prescribed, on the side boundaries v_x is prescribed and v_y is periodic, and the upper boundary is left free. The scale in the x and y directions, non-dimensionalized against the layer thickness, is the same for all plots and given in (a3).

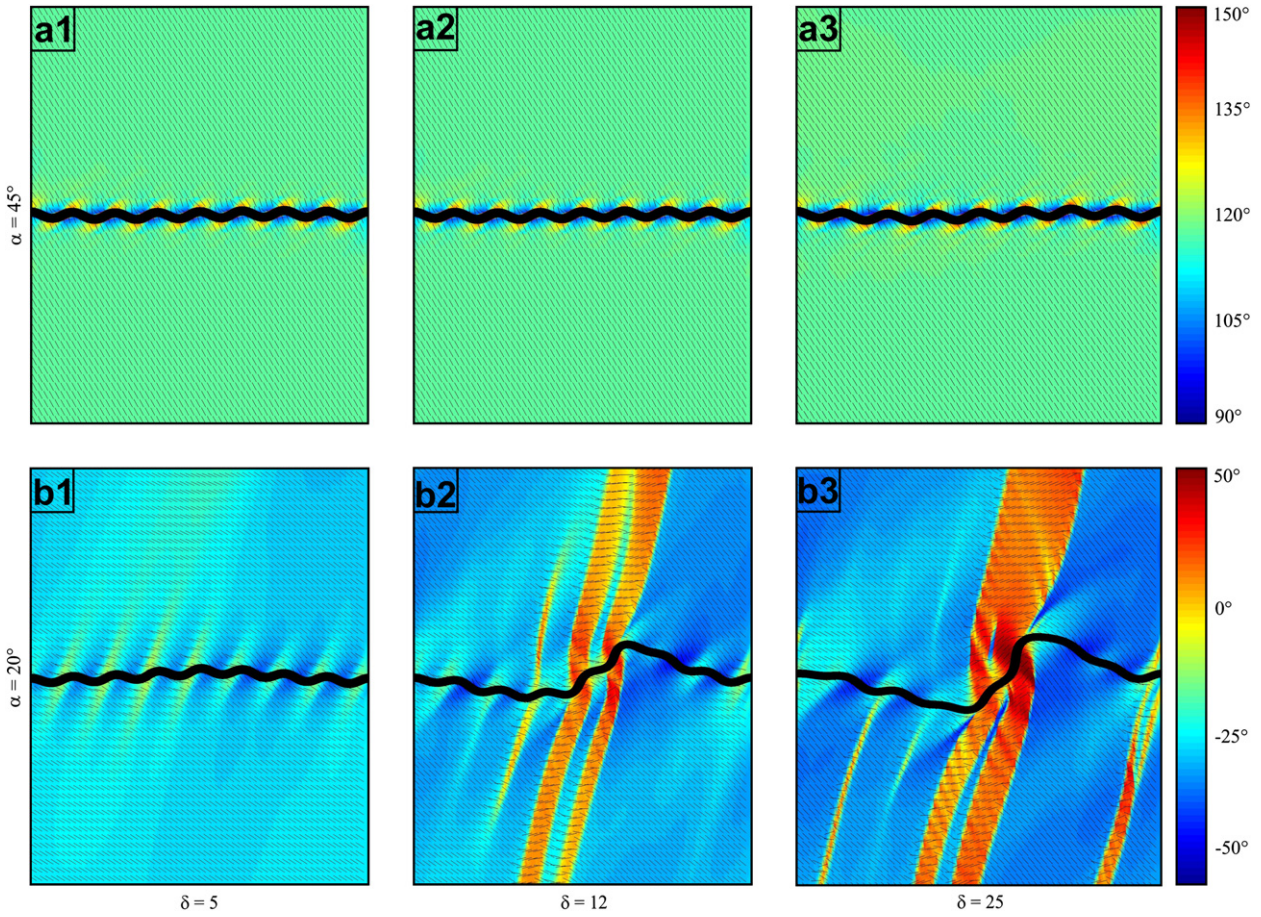

Fig. 5. Colour-coded plots of the orientation of the anisotropy planes and the finite fold shape after 32% of layer-parallel pure shear shortening in linear viscous material (viscosity contrast $\mu_c = 10$), for matrix anisotropy degrees of $\delta = 5$, 12 and 25. (a1–a3): initial anisotropy orientation at 45° to the competent layer; (b1–b3): anisotropy initially oriented at 20° (sub-parallel to the layer). Boundary conditions and angular conventions are the same as in Fig. 4, as are the x and y dimensions as given in Fig. 4a3.

determined by the width of the model and is obviously linked to the development of asymmetric chevron folds in the matrix.

Figs. 4 and 5 illustrate the strong influence that a more obliquely oriented planar anisotropic matrix (i.e. $\alpha \neq 0°, 45°$ or 90°) exerts on the shape of the finite fold in a Newtonian material and provides interesting insights into the kind of geometry that one might expect to find in natural rocks if anisotropy plays a role. In particular, it is important to note that the asymmetric chevron fold in the matrix in Fig. 5b2–b3, did not develop due to a simple shear component of the bulk deformation field, but because the matrix anisotropy was initially oriented at an oblique angle to the competent layer. It is also notable that, although the initial growth rates at very small amplitude are the same for $\alpha = 20°$ and 70° (Fig. 1), the finite amplitude folds that develop are markedly different. This is because, for $\alpha = 20°$, finite amplitude folding in the matrix progressively rotates the local plane of anisotropy into an orientation with an increasing shear component, which causes geometric softening and promotes fold growth, whereas this is not the case for the 70° orientation.

As noted above, the top boundary condition was a free surface in all the experiments presented in Figs. 4 and 5. Such a set-up would be comparable in nature to folding reaching to the earth's surface (also a free boundary) or confined on one side by a weak layer. If the boundaries are located far enough from the single layer, their influence is negligible in isotropic materials, and the setup then provides very accurate results in benchmarking tests (e.g. see Fig. 2a of Kocher et al., 2006). However, when looking at the deformation of the whole model domain in the models for anisotropic material presented here (which is in fact much larger than the selected regions close to the layer shown in Figs. 4 and 5), it becomes clear that the matrix structures (i.e. the chevron folds, Fig. 5b2–b3) stretch across the whole domain and reach the boundaries. In fact, the free surface at the top of these models is still strongly deformed (Fig. 6). This observation suggests that the boundary conditions in anisotropic Newtonian models have a stronger influence on the finite deformation in the centre of the model than is the case for isotropic material. Indeed, this is well seen in Fig. 6, where the location of the chevron fold band responsible for the developing asymmetry of the larger wavelength secondary fold is clearly related to the corner of the model. Indirectly, this is also confirmed by another experiment with fixed velocities v_x and v_y instead of a free surface at the top boundary for the same setup as in Fig. 5b2. This experiment failed, with the iteration to maintain incompressibility not converging because of the added constraint that the fixed boundary placed on the anisotropic material as it attempted to buckle at the boundary. The effects of boundary conditions and their influence on the development of asymmetric folds related to inclined anisotropy are discussed further in Section 6 below.

5. Anisotropy and non-linearity

Based on experimental data gained from natural rock samples, it is commonly argued that rock deformation is more accurately described by power-law constitutive equations (with stress exponent n between 3 and 5) rather than by a linear viscous (Newtonian) rheology (e.g. Ranalli, 1995; Turcotte and Schubert, 2002). Some aspects of the interplay between anisotropy and non-linear

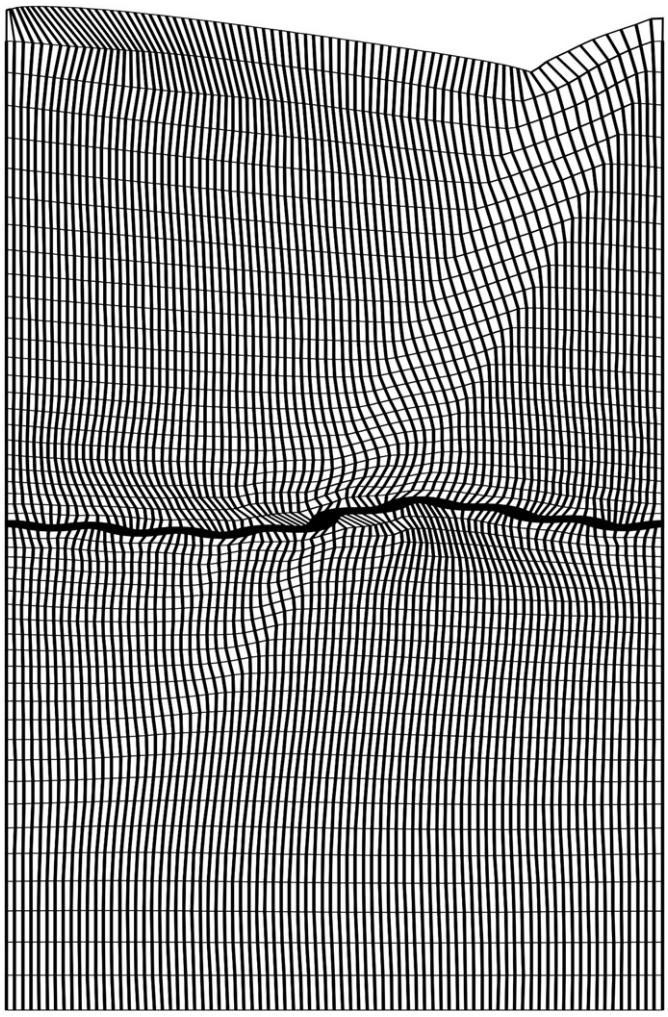

Fig. 6. Marker grid showing the entire model domain deformation for the experiment in Fig. 5b2, with the vertical axis reduced in scale by a factor of 3. Note that the free surface at the top of the model is strongly deformed.

rheology, e.g. the tendency to form conjugate kink-bands, were already discussed in Kocher et al. (2006). Fletcher (2005) recently presented an analytical investigation of instability development in an anisotropic power-law fluid. He considered a homogeneous (i.e. without any distinct single layer) anisotropic material of infinite extent, for which there are clearly no boundary effects. However, in numerical and analogue models (and in nature) there will always be boundaries, and non-linearity also plays an important role in the attenuation of boundary effects by providing a mechanism of localization. This is demonstrated by two experiments (Fig. 7a,b) that correspond in their general setup to the experiments b2 in Figs. 4 and 5, except that both matrix and layer have a power-law rheology (stress exponent $n = 3$), there is no free upper surface, and two different upper and lower boundary constraints are compared. In Fig. 7a,b, the velocities v_x and v_y on the upper and lower boundaries are fully constrained but two control experiments confirmed that the resulting finite fold geometry is independent of the boundary conditions applied at the top of the model (for example the result is effectively identical if the lower boundary is fully constrained but the upper boundary is left free, as in Figs. 4–6). For comparison, in Fig. 7c,d, v_y is constrained on the upper and lower boundaries, but v_x is not (i.e., a free slip condition). The influence of this change in boundary conditions is discussed in Section 6.

For a sub-perpendicular anisotropy ($\alpha = 70°$, Fig. 7a), the geometry developed for a power-law rheology is not dramatically different to that observed in the corresponding experiment for Newtonian materials (Fig. 4b2). As would be expected, the amplitude of the folds in the single layer is larger, reflecting the larger growth rate in non-linear materials for the same effective viscosity contrast (Fletcher, 1974; Smith, 1977). However, for both Newtonian and power-law rheology, the deformation is concentrated near the single layer and there is no tendency for larger scale folding in the matrix.

In contrast, for the case of an anisotropy that was initially subparallel to the layer (Fig. 7b), the resulting folds in the competent layer are markedly different from those observed in the corresponding experiment with Newtonian materials (Fig. 5b2). The layer is folded regularly into folds of a wavelength that is governed by the initial perturbation wavelength. A second order folding of the layer, as observed in the corresponding Newtonian experiments, is largely absent. The matrix is deformed into asymmetric chevron folds, the axial planes of which are spaced at roughly the wavelength of the folded competent layer. A single large chevron fold that reaches as far as the free surface (as was found in the Newtonian material) is absent, and the deformation is spread more regularly throughout the matrix. This observation is counter-intuitive at first sight, because a stronger localization is expected in non-linear material. However, the tendency for the heterogeneous deformation to be more localized around the single layer means that the perturbed flow does not reach to the boundaries and therefore is less influenced by boundary effects (e.g. whether the upper boundary is free or constrained). The clear influence of the free upper boundary on the development of the larger wavelength asymmetric fold as seen in Figs. 5b and 6 for Newtonian materials is therefore not observed in the power-law example of Fig. 7b, irrespective of whether the upper boundary is free or fully constrained. However, differences are observed when the velocities on the lower boundary are also no longer fully prescribed (Fig. 7c,d) and these effects will now be discussed.

6. Effect of slip boundary conditions

Compared to analogue experiments, numerical experiments have the advantage that boundary conditions can be more strictly defined. As noted in the previous section, power-law rheology provides a mechanism to damp boundary effects by promoting localization of deformation. However, the influence of boundary conditions on the resulting structure can be considerable, even for power-law rheology.

The two experiments in Fig. 7c,d show the difference that free slip boundary conditions can make if anisotropy plays a role. They correspond in their setup to the experiments in Fig. 7a,b with the difference that v_y is prescribed and v_x is unconstrained at the top and bottom boundary. In contrast, in Fig. 7a,b both v_x and v_y are prescribed at the lower boundary (and the upper boundary constraint in this case is found to have little influence, whether free or constrained). The resulting folds in Fig. 7c,d show a large second wavelength equal to the width of the model domain. This second wavelength is characterized by an anticlockwise (c) or clockwise (d) rotation of the central part of the competent layer with respect to its initial orientation. The absence of shear stress at the top and bottom boundaries allows this rotation, which passively folds the competent layer. It is important to note that the larger wavelength only occurs because of the imposed vertical velocity being periodic at the lateral boundaries. Without this constraint, matrix and layer would rotate as a whole. These experiments establish that: (1) power-law rheology is a means to reduce some, but not all, boundary effects; (2) the interplay between rheology, initial domain geometry and applied boundary conditions is complex; and (3) a tight control on boundary conditions is of particular importance if the material

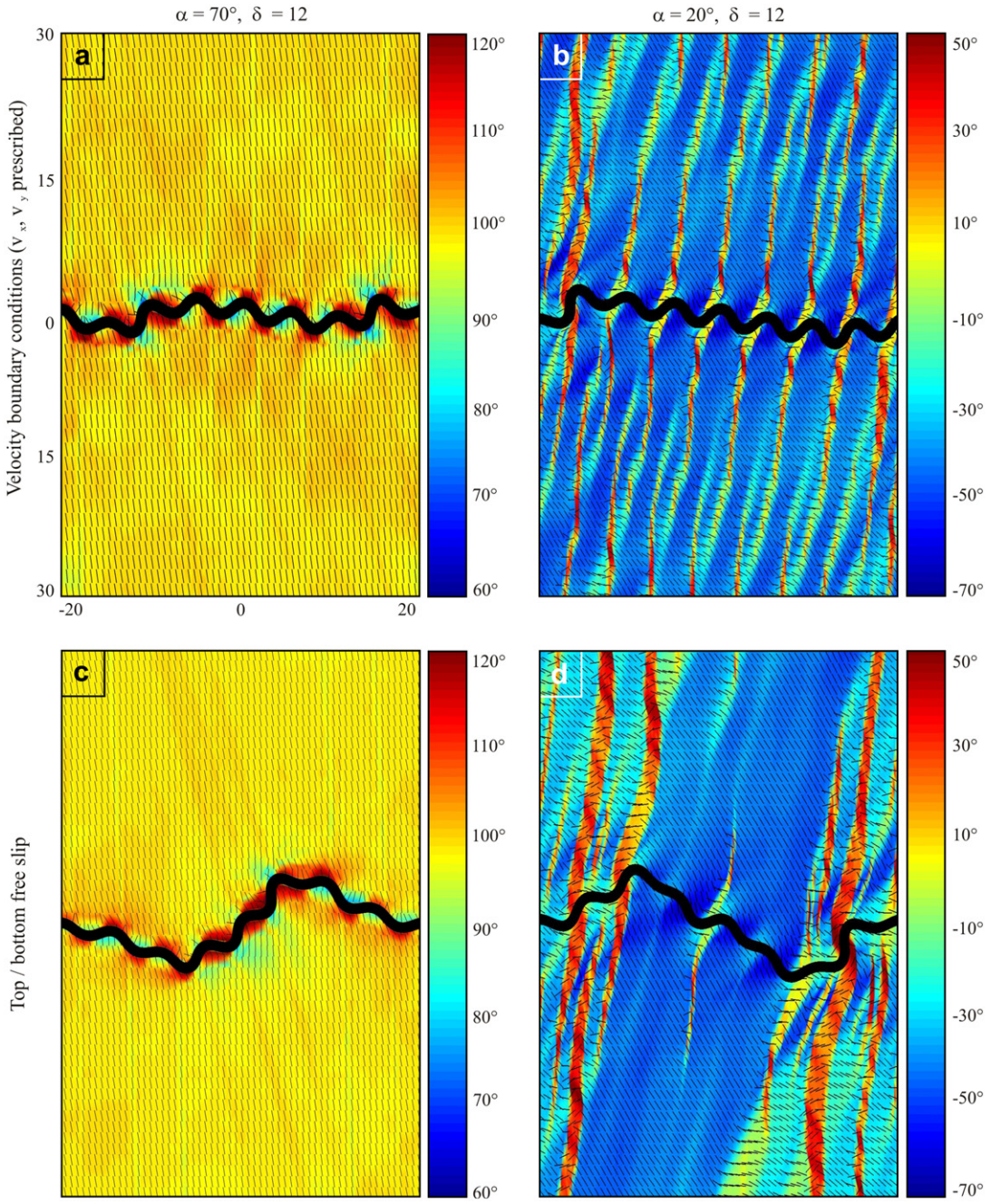

Fig. 7. Colour-coded plots of the orientation of the anisotropy planes and the finite fold shape after 32% of layer-parallel pure shear shortening in power-law material ($n = 3$), for an anisotropy degree of $\delta = 12$. The viscosity contrast was $\mu_c = 10$ in all experiments. The initial angle α between the layer and the anisotropy plane was 70° (sub-perpendicular) to the competent layer for (a) and (c), and 20° (sub-parallel) to the layer for (b) and (d). In (a) and (b), all boundary velocities are prescribed with the exception of v_y at the lateral boundaries, which is periodic, but unconstrained otherwise. In (c) and (d), only the velocities normal to the boundary are given, with the exception of the lateral boundary-parallel velocities, which are periodic, but unconstrained otherwise. Angular conventions as in Fig. 4.

under consideration is anisotropic and particularly if the plane of anisotropy is at a small oblique angle to the boundaries.

7. Asymmetric kink-bands and chevron folds in anisotropic power-law material

As discussed by Kocher et al. (2006), symmetric chevron folds developed in a matrix with power-law rheology can evolve from symmetric conjugate kink-bands through a process of kink-band broadening and merging. If the anisotropy is initially oriented obliquely to the competent layer, a similar process takes place, but with some important differences. This is demonstrated in Fig. 8a–d, which shows a series of deformation stages of the same experiment as in Fig. 7b (where $\alpha = 20°$).

As in the case of a layer-parallel anisotropy, buckling in the competent layer triggers an internal instability in the anisotropic matrix, which experiences a shortening component parallel to its plane of anisotropy. The first noticeable indications of deformation in the matrix are the rotated planes of anisotropy outlined by the dark blue bands in Fig. 8a. These deformation bands form perpendicular to the anisotropy planes, and not at an angle of 15°–20°, as kink-bands did in the case of a layer-parallel anisotropy (Kocher et al., 2006). Instead, their orientation with respect to the anisotropy resembles that of the chevron folds that were observed to develop in Newtonian

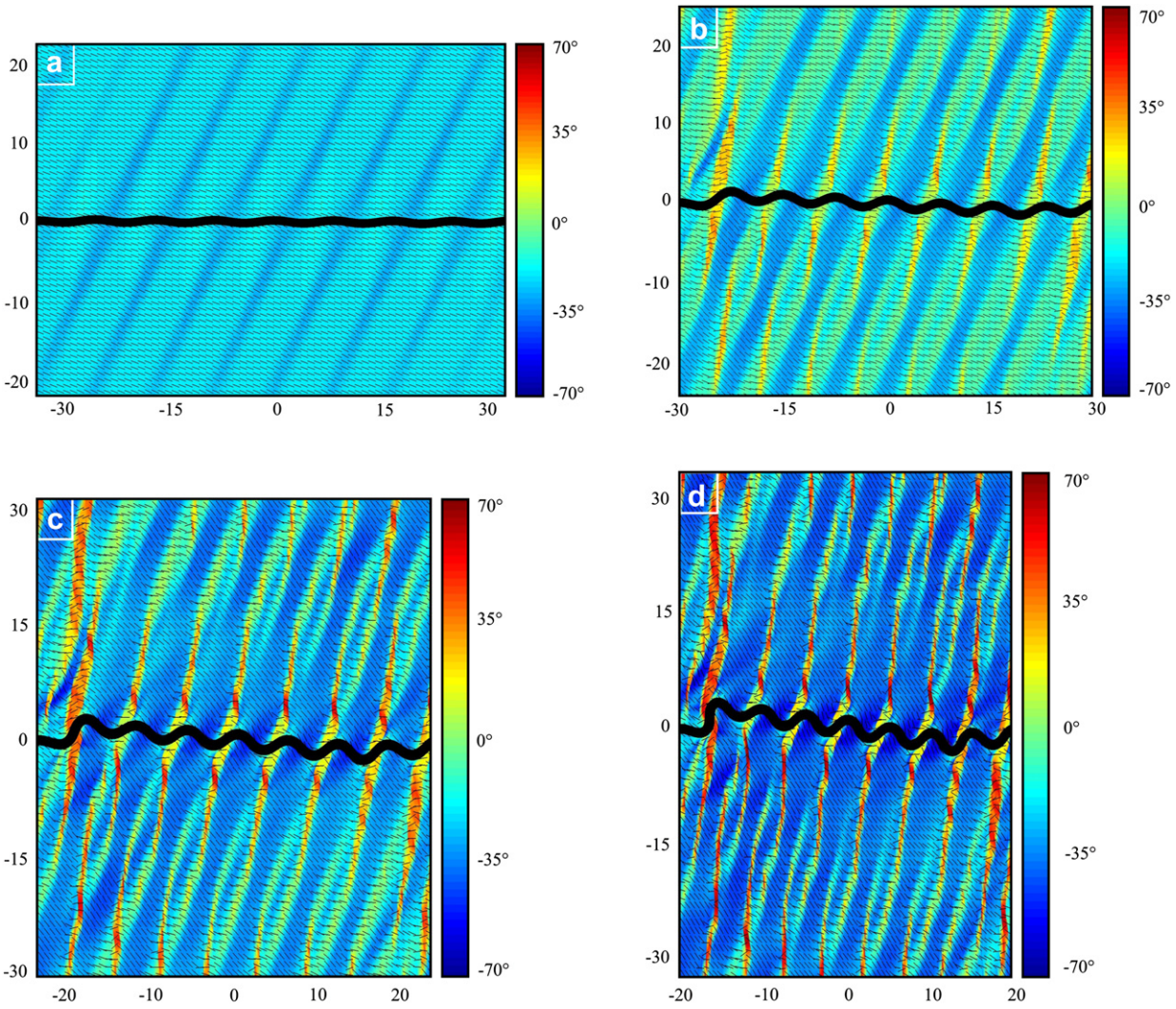

Fig. 8. Colour-coded plots of the anisotropy orientation and finite fold shapes for an isotropic power-law layer ($n = 3$) embedded in anisotropic power-law matrix ($n = 3$, $\delta = 12$), at (a) 8%, (b) 19%, (c) 27%, and (d) 35% bulk pure shear shortening. The initial angle between the anisotropy and the competent layer was $\alpha = 20^\circ$. The first set of deformation bands (dark blue areas in a) develops perpendicular to the planes of anisotropy, whereas the second (conjugate) set (orange deformation bands in b) develops at an angle of about 15° to the planes of anisotropy. Angular conventions as in Fig. 4.

material, the axial planes of which were also perpendicular to the anisotropy orientation. The second set of deformation bands starts to form at later stages of deformation (Fig. 8b, yellow–red band-like structures), and makes an angle of 15°–20° to the anisotropy plane. This corresponds to the kink-band orientations observed in the case of a layer-parallel anisotropy. It is interesting to note that the width of the two types of band-like structures is rather different. The second set of bands is much narrower than the first and does not cross the latter. It therefore remains much more limited in extent.

During progressive deformation, the two sets of deformation bands broaden and merge to form asymmetric chevron folds, as can be seen in the close-up view of the central parts of Fig. 8b,d shown in Fig. 9. The asymmetry of the chevron folds and the kink-band-like structures is caused by the oblique anisotropy orientation, and not by any shearing component to the background deformation field. It is important to note that the folds in the competent layer remain largely symmetric throughout the entire deformation process.

8. Random initial perturbations – a closer approximation to natural conditions

The previous experiments assumed a sinusoidal initial perturbation of the single layer interface, with an initial wavelength corresponding to the fastest growing or 'dominant' wavelength for the isotropic Newtonian problem. Under natural conditions, both the perturbation of the layer-matrix interfaces and the anisotropy orientation are more likely to show a random variation around an average orientation. Perfect homogeneity in the anisotropy orientation causes the developing chevrons to become (too) regular compared with natural examples, because no material inhomogeneities inhibit the propagation of the initial perturbation of the layer interface into the matrix.

Fig. 10 shows a single layer fold and the surrounding matrix structure that result if the anisotropy orientation is initially randomly perturbed by $\pm 1^\circ$ around an average α of 20° and the layer interface is perturbed with a random red noise signal (which is different for the top and bottom interface). Note that the viscosity contrast between matrix and layer is still $\mu_c = 10$. The resulting single layer fold has a much larger wavelength and amplitude compared to the previous experiments, an observation that is in agreement with the prediction of larger growth rates and longer wavelengths for anisotropic materials as seen in Fig. 1. More interesting, however, is that the central individual folds of the competent layer are clearly asymmetric. Toward the lateral boundaries, the asymmetry disappears because v_x is prescribed there as a boundary condition. The random perturbation of the anisotropy orientation in the matrix has

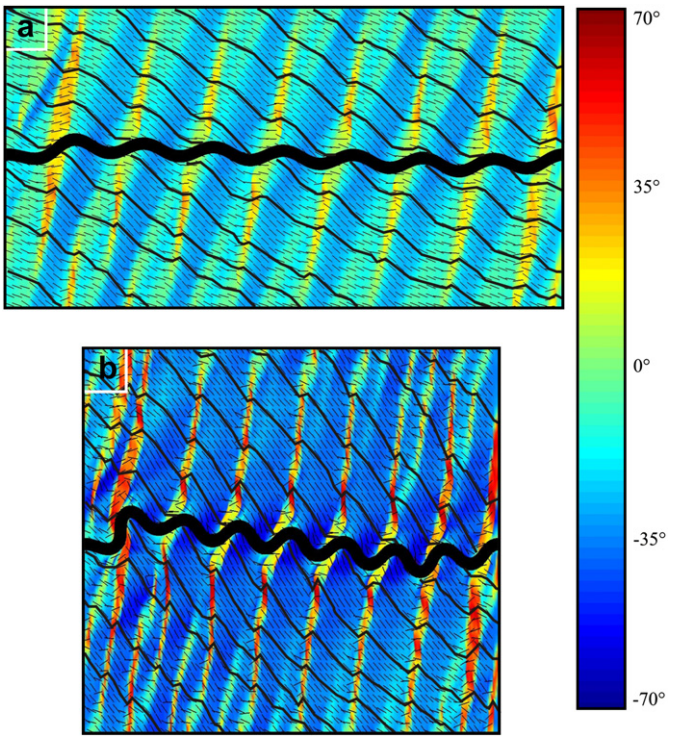

Fig. 9. Enlarged colour-coded plots of anisotropy orientation and finite fold shape at (a) 15% and (b) 32% shortening of a power-law layer embedded in anisotropic material ($n = 3$, $\delta = 12$, the same experiments as in Fig. 8b,d). The solid black lines trace the approximate anisotropy orientation. The asymmetric deformation bands visible at 15% shortening (note the wide dark blue areas – that developed first – compared to the narrow orange bands) are mostly merged into asymmetric chevron folds at 32% shortening. The asymmetry in the matrix chevron folds occurs due to the anisotropy not being oriented parallel to the direction of maximum compression at the onset of deformation.

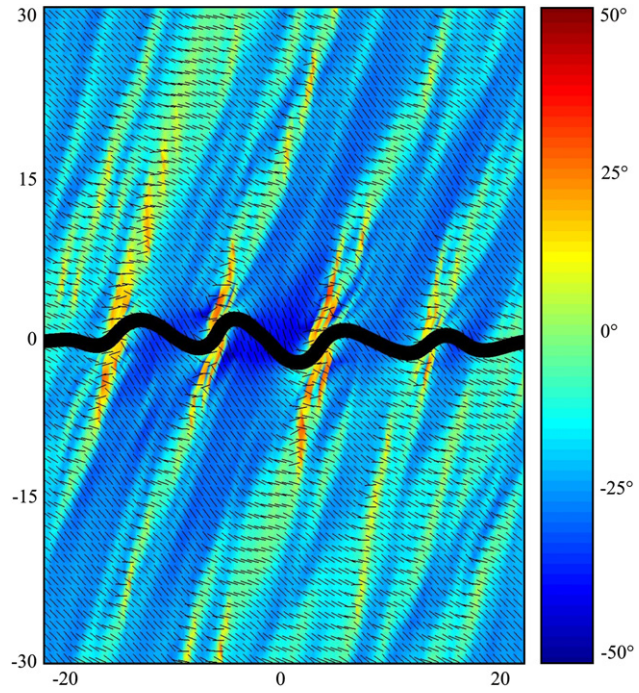

Fig. 10. Colour-coded plot of the anisotropy orientation and finite fold shape at 28% shortening of a power-law layer ($n = 3$) embedded in anisotropic matrix ($n = 3$, $\delta = 6$), subjected to a layer-parallel homogeneous pure shear background deformation. All boundary velocities are prescribed except the vertical velocities at the lateral boundaries, where v_y is periodic, but unconstrained otherwise. The layer interface was perturbed with a red noise random signal (maximum amplitude = 5% of the layer thickness), and the anisotropy orientation varied randomly ±1° around an average initial orientation of $\alpha = 20°$. Angular conventions as in Fig. 4.

two effects. (1) It leads to local matrix instabilities that are not triggered and governed by spreading of the perturbation in the competent layer interface, but by the local perturbation wavelength within the matrix. (2) As a consequence, the layer-induced perturbations can no longer propagate as extensively through the matrix, because they interfere with the local instabilities in the matrix, which causes a more irregular (and more naturally-looking) finite deformation pattern.

These results demonstrate that asymmetric folds are to be expected in anisotropic material in both layer and matrix, even if the background deformation field is purely coaxial, the degree of anisotropy is low, the perturbations in layer and matrix are random, and the competent layer is initially oriented parallel to the maximum shortening direction.

9. Discussion

The results presented here illustrate the influence of an arbitrarily oriented matrix anisotropy on the finite shape of a fold in a single isotropic competent layer under pure shear bulk deformation. These new numerical experiments provide additional insights into the deformation process in anisotropic materials that were not obtained in our previous investigation of folding of a competent layer in a matrix with layer-parallel anisotropy (Kocher et al., 2006).

The growth rate spectra establish that the analytical solution of Fletcher (1974), combined with the earlier work of Biot (1965), predicts growth rates that correspond well with the numerical results for orientations of the plane of anisotropy at 0°, 45° or 90° to the layer (at least if the normal viscosity contrast between the layer and the matrix is high; Fig. 1a–c). The description of the bulk viscosity of the matrix as $\mu = \sqrt{\mu_n \mu_s}$, as proposed by Biot (1965), corresponds to a (geometric) mean stiffness of the anisotropic material. As shown by Cobbold (1976), μ is also the determinant of the constitutive matrix that links stresses and strain rates in an anisotropic viscous matrix. This determinant is insensitive to an exchange of μ_s and μ_n in the system of equations that occurs if an anisotropic material is rotated 45°, which explains the equality of the growth rates at 0°, 45° and 90°. While the numerical growth rates for anisotropies at 45° are also in good agreement with the analytical values at low viscosity contrasts, the growth rates for $\alpha = 0°$ and 90° show considerable misfit for large anisotropy values, the origin of which however could not be determined (Fig. 1d–f). These results demonstrate that the analytical solution of Fletcher (1974) can indeed be used as a benchmark test for numerical codes in the case of a symmetric anisotropy orientation (at 0°, 45° or 90° to the layer), provided that the viscosity contrast between layer and matrix is sufficiently large.

However, the numerical growth rates for oblique anisotropies ($\alpha \neq 0°$, 45° or 90°) deviate strongly from the analytical solution (Fig. 1d–f). Possible explanations for this behaviour are not straightforward and show the limits in applicability of the analytical single layer folding theory. An oblique anisotropy orientation implies that the mechanical properties of the matrix will be different on opposing limbs of a growing fold. This difference causes one limb to grow faster, while the amplification of the second limb is hampered. In addition, folding in a Newtonian anisotropic matrix involves strong rotational effects (Fig. 5b2–b3). If this potential rotational component is damped by prescribing non-rotational boundary conditions (e.g. by setting v_y to be periodic on the lateral boundaries), the growth rate of folding is correspondingly reduced (e.g. see (4) and (5) in Fig. 3). Such boundary conditions were

necessary in the numerical models of finite amplitude folding in order to counteract the tendency for the whole model to rotate. Single layer folding developed in an oblique anisotropic matrix involves complex displacements of the layer surface. The perturbation flow field is not as simple as for single layer folding in an isotropic material (e.g. see Passchier et al., 2005, Fig. 10), but involves a combination of layer-perpendicular and layer-parallel motion, together with a considerable amount of layer rotation. Because of this, it is not possible to generalize the current results to make any statement about wavelength selection or growth rate trends. Due to the complex kinematics, it will also be very difficult, if not impossible, to deduce viscosity contrasts from folds (Sherwin and Chapple, 1968; Schmalholz and Podladchikov, 2001) when an oblique anisotropy is present in the matrix.

As discussed above, if there are neither irregularities in the initial anisotropy orientation nor non-linear rheological effects, the final fold shape is strongly influenced by the interaction of matrix deformation with the boundaries of the model domain, irrespective of how far they are located from the competent layer. The asymmetry and second-order folding of larger wavelength that occurred in Newtonian material (b3 in Figs. 4 and 5) are entirely caused by the interaction of the free surface at the top of the model with the deforming anisotropic matrix. In natural rocks, however, material properties can vary considerably (e.g. Kim and Gao, 1995) and the rheology often follows a non-linear constitutive law (e.g. Ranalli, 1995). The inclusion of these factors in numerical experiments is necessary to provide a mechanism for more distributed deformation in the matrix, leading to the formation of less pervasive, less regular, but more natural structures.

Furthermore, the results emphasize the special role of the boundary conditions in numerical and analogue experiments that deal with anisotropic material. Besides the effects of different kinds of boundary conditions (stress or velocity prescribed), the type of boundary condition (free slip, prescribed velocity) has a much stronger influence on the result if the anisotropy is oblique to the principal stress axes. Any slip at the boundaries will allow the matrix and layer to rotate as a whole. This is of particular importance to analogue models, where perfect non-slip boundary conditions are difficult to achieve. Even for power-law materials, where the effect of the boundaries is reduced by the tendency to localize deformation around the perturbed region of folding, there is a distinct difference between free-slip and non-slip boundaries (Fig. 7). In our experiments, free slip upper and lower boundary conditions allow more internal rotation than totally prescribed boundaries and therefore also the development of a second order fold with wavelength equal to the model width, although without any clear asymmetry (Fig. 7d). Such rotational effects developed when a non-slip boundary condition is not strictly imposed will also complicate rock deformation laboratory experiments that attempt to determine the degree of anisotropy in natural rocks by compressing samples at different angles to the foliation.

The experiments in power-law material document the formation of asymmetric chevron folds in anisotropic matrix by broadening and merging of conjugate deformation band structures. The two sets of deformation bands develop neither symmetrically nor simultaneously with respect to the oblique anisotropy, and also differ in their width. In the set of bands that develops first, the sense of rotation of the anisotropy planes is the same as that imposed by the bulk pure shear background deformation, whereas in the second set it is opposite. The first set of bands is favoured because it rotates the plane of anisotropy into an orientation at a higher angle to the maximum shortening direction, which in turn causes a local reduction of the stresses in the direction of shortening (Cobbold, 1976). An antithetic rotation of the anisotropy planes increases the stresses parallel to the maximum shortening direction. This 'resistance' has to be overcome to develop the second-antithetic-set of bands, which are therefore more difficult to form. The observed variations in angle (with respect to the plane of anisotropy) and width correspond well with the analogue experiments of Cobbold et al. (1971, Fig. 17). The conjugate deformation bands show characteristics of both chevron folds and 'true' kink-bands. An unambiguous classification of structures as either of these two end-members is therefore not always possible, and transitional stages between them are likely to be formed in natural rocks (as suggested, for example, by Treagus, 2003).

The combination of a random initial perturbation on the layer-matrix interface and an oblique anisotropy orientation in the matrix produces large wavelength to thickness folds despite the low normal viscosity contrast (Fig. 10). This is consistent with the increase in growth rate and wavelength predicted from the growth rate spectra at infinitesimal wavelength for such anisotropic behaviour (shown in Fig. 1 for the linear viscous case, but also applicable for power-law rheology). The developing single layer folds are now asymmetric, even though the background deformation field is purely coaxial. As discussed before, the asymmetric chevron folds in the matrix are a consequence of the different widths of the conjugate deformation bands, which is induced by the initially oblique anisotropy. Additional experiments, the results of which are not presented here, show that the asymmetry of the single layer fold depends to some degree on the normal viscosity contrast between layer and matrix. At higher viscosity contrasts, very irregular fold shapes with large amplitudes are developed due to the high growth rates and the strong interaction with the matrix. Periodic fold trains with a recognizable asymmetry in the competent layer are more clearly developed if the viscosity contrast between layer and matrix is low.

These experiments with an initial random perturbation, which in our opinion most closely approximate natural conditions, demonstrate that asymmetric folds can form in coaxial flow fields as a result of interaction between a competent isotropic layer and an anisotropic matrix. A sequence of kinematically distinct deformation phases (as often suggested, for example, by Carosi et al., 2004) is not required to form asymmetric folds in anisotropic rocks.

10. Conclusions

The orientation of the matrix anisotropy around a single isotropic layer has strong effects on the infinitesimal and finite stages of folding of that layer. If the bulk viscosity is approximated as the geometric mean of the normal and shear viscosities, the (isotropic) analytical solution of Fletcher (1974) can be numerically reproduced for specific anisotropy orientations (i.e. $\alpha = 0^\circ$, 45° or 90°) and high normal viscosity contrasts. The best correspondence between numerical models and the analytical solution, for both low and high normal viscosity contrasts, is with $\alpha = 45^\circ$. A careful use of the analytical solution for benchmarking of numerical code including anisotropic behaviour is therefore possible. For other orientations of the planar matrix anisotropy, the dynamic growth rate of the single layer fold differs from the analytical value, particularly for lower normal viscosity contrasts and obliquities (e.g. $\alpha = 20^\circ$ or 70°), probably reflecting the marked asymmetry of the folds developed in the matrix, with opposite limbs in a quite different orientation relative to the bulk shortening direction.

Strict control of the boundary conditions in both analogue and numerical experiments is crucial when dealing with anisotropic materials, especially when the plane of anisotropy is oblique to the boundaries, because the anisotropic domains tend to rotate if this is allowed by free-slip conditions at the boundaries. This bulk rotation can strongly influence the finite structures. In non-linear materials, the matrix deformation is characterized by the formation of conjugate deformation bands, which develop neither simultaneously nor symmetrically. The asymmetry of these conjugate bands produces asymmetric chevron folds as a result of broadening and

merging of the bands during progressive deformation. Likewise, folded isotropic competent layers in a weak matrix with a randomly perturbed anisotropy orientation can show a significant asymmetry at low viscosity contrasts. We conclude that asymmetric folds in both matrix and layer can be formed in anisotropic rock subjected to pure shear bulk deformation, even if the degree of anisotropy is low and the competent layer is initially oriented parallel to the maximum shortening direction.

Acknowledgements

Thorough and very helpful reviews from D. Schmid and P. Cobbold, which significantly improved the revised version, are gratefully acknowledged. This study was supported by ETH project 0-20998-02.

References

Biot, M.A., 1965. Mechanics of Incremental Deformations. John Wiley and Sons, Inc., New York.
Carosi, R., Iacopini, D., Montomoli, C., 2004. Asymmetric fold development in the Variscan Nappes of central Sardinia (Italy). Comptes Rendus Geoscience 336, 939–949.
Cobbold, P.R., 1976. Mechanical effects of anisotropy during large finite deformations. Bulletin de la Société Géologique de France 18, 1497–1510.
Cobbold, P.R., Cosgrove, J.W., Summers, J.M., 1971. Development of internal structures in deformed anisotropic rocks. Tectonophysics 12, 23–53.
Cuvelier, C., Segal, S., van Steenhoven, A., 1986. Finite Element Methods and Navier–Stokes Equations. D. Reidel Publishing Company, Dordrecht, Holland.
Fletcher, R.C., 1974. Wavelength selection in folding of a single layer with power-law rheology. American Journal of Science 274, 1029–1043.
Fletcher, R.C., 2005. Instability of an anisotropic power-law fluid in a basic state of plane flow. Journal of Structural Geology 27, 1155–1167.
Kim, K., Gao, H., 1995. Probabilistic approaches to estimating variation in the mechanical properties of rock masses. International Journal of Rock Mechanics and Mining Sciences and Geomechanics Abstracts 32, 111–120.
Kocher, T., 2006. FLASH code description. Available at: http://e-collection.ethbib.ethz.ch/cgi-bin/show.pl?type=bericht&;nr=459.
Kocher, T., Schmalholz, S.M., Mancktelow, N.S., 2006. Impact of mechanical anisotropy and power-law rheology on single layer folding. Tectonophysics 421, 71–87.
Latham, J.-P., 1985a. The influence of nonlinear material properties and resistance to bending on the development of internal structures. Journal of Structural Geology 7, 225–236.
Latham, J.-P., 1985b. A numerical investigation and geological discussion of the relationship between folding, kinking and faulting. Journal of Structural Geology 7, 237–249.
Mühlhaus, H.-B., Dufour, F., Moresi, L., Hobbs, B., 2002a. A director theory for viscoelastic folding instabilities in multilayered rock. International Journal of Solids and Structures 39, 3675–3691.
Mühlhaus, H.-B., Moresi, L., Hobbs, B., Dufour, F., 2002b. Large amplitude folding in finely layered viscoelastic rock structures. Pure and Applied Geophysics 159, 2311–2333.
Passchier, C.W., Mancktelow, N.S., Grasemann, B., 2005. Flow perturbations: a tool to study and characterize heterogeneous deformation. Journal of Structural Geology 27, 1011–1026.
Poliakov, A., Podladchikov, Y., 1992. Diapirism and topography. Geophysical Journal International 109, 553–564.
Ranalli, G., 1995. Rheology of the Earth, second ed. Chapman and Hall, London.
Schmalholz, S.M., Podladchikov, Y.Y., 2001. Strain and competence contrast estimation from fold shape. Tectonophysics 340, 195–213.
Schmid, D.W., Podladchikov, Y.Y., 2003. Analytical solutions for deformable elliptical inclusions in general shear. Geophysical Journal International 155, 269–288.
Sherwin, J.A., Chapple, W.M., 1968. Wavelengths of single layer folds: a comparison between theory and observation. American Journal of Science 266, 167.
Smith, R.B., 1975. Unified theory of the onset of folding, boudinage and mullion structure. Geological Society of America Bulletin 86, 1601–1609.
Smith, R.B., 1977. Formation of folds, boudinage, and mullions in non-Newtonian materials. Geological Society of America Bulletin 88, 312–320.
Treagus, S.H., 2003. Viscous anisotropy of two-phase composites, and applications to rocks and structures. Tectonophysics 372, 121–133.
Turcotte, D.L., Schubert, G., 2002. Geodynamics, second ed. Cambridge University Press.
Viola, G., Mancktelow, N.S., 2005. From XY tracking to buckling: axial plane cleavage fanning and folding during progressive deformation. Journal of Structural Geology 27, 409–417.